Quasi-Static and High Strain Rate Simple Shear Characterization of Soft Polymers



K. Upadhyay¹ · A. Bhattacharyya² · G. Subhash¹ · D.E. Spearot¹

Received: 19 November 2018 / Accepted: 1 April 2019 © Society for Experimental Mechanics 2019

Abstract

The simple shear response of soft polymers under large deformation (>50%) and strain rates spanning $10^{-3} - 10^{3}$ s⁻¹ is characterized by developing quasi-static and split-Hopkinson pressure bar based single-pulse dynamic simple shear experiments rooted in continuum mechanics fundamentals. Cross-linked polydimethylsiloxane (PDMS) is chosen as a model material. By examining the evolution of stress, strain and strain rate, the latter two parameters measured using two-dimensional digital image correlation (DIC), it is demonstrated that dynamic simple shear deformation consists of four distinct stages: momentum diffusion, inertia effect, steady-state material response, and strain rate decay. By isolating the unsteady and steady-state deformation stages, inertia-free material response is captured under a uniform strain rate. It is shown that the shear response of PDMS is nearly linear with a weakly rate-sensitive shear modulus in the investigated strain rate range. Further, by analyzing the DIC strain-field and comparing the kinematic experimental results with those predicted by classical continuum mechanics, it is demonstrated that the proposed experiments not only achieve a nearly theoretical simple shear state that is uniform across the specimen, but also allow for post-test validation of individual experiments based on these criteria.

Keywords PDMS · Simple shear · Large deformations · Strain rate sensitivity · Split-Hopkinson pressure bar (SHPB) · Digital image correlation (DIC)

Introduction

Reliable and accurate mechanical characterization of biological tissues and soft polymers is essential for the design and development of tissue phantoms, scaffolds, and biomedical implants, as well as for the formulation of computational models of human organ tissues. The latter have been extensively used to conduct surgical planning and training, to design protective equipment, and to study extreme events such as ballistic impact, blast, automobile crashes, and conditions such as cancer and traumatic brain injury (TBI) [1–7]. Such events involve a wide range of loading conditions, strain rates $(10^{-1}-10^3 \text{ s}^{-1})$ and large deformations [8–12], which

☑ G. Subhash subhash@ufl.edu

Published online: 22 April 2019

highlights the need for high fidelity experimental data in the development of effective constitutive relationships.

Existing literature on soft polymers mainly consists of their uniaxial compression [13–17] and tension [18–20] responses under a range of strain rates, which have been further used to develop constitutive relations generally based on hyperelasticity and/or viscoelasticity principles [21–23]. This sole consideration of uniaxial deformation, although relatively easy and convenient from an experimental standpoint, can lead to inaccurate results when applied to complex realworld deformation modes involving tri-axial loading and large deformations. It has been suggested that test data under three primary deformation modes: compression, tension and shear, are required for the estimation of hyperelastic model constants [24, 25], a recommendation that has been recently shown to be necessary to ensure thermodynamic stability of many hyperelastic strain energy density functions [26]. The majority of literature on shear deformation consists of oscillatory tests such as dynamic mechanical analysis (DMA) and shear rheometry, among others [27–32]. Although useful in certain strain/strain rate ranges, these oscillatory tests have major limitations: (i) very small strains are achieved in the high frequency regime, (ii) strain rates are limited to $\sim 10^2 \text{ s}^{-1}$, and more



Department of Mechanical and Aerospace Engineering, University of Florida, Gainesville, FL 32611, USA

Department of Metallurgical and Materials Engineering, Indian Institute of Technology Jodhpur, Karwar, Rajasthan 342037, India

importantly, (iii) the oscillatory shear deformation does not simulate common impact scenarios (blast injury, crash, fall, etc.), which are single pulse in nature and induce large complex deformations at high strain rates [33, 34].

A few single-pulse simple shear tests have been reported in the literature, mainly using torsion or single/double lap testing configurations. Pasumarthy and Tippur [35] used full-field 2D digital image correlation (DIC) and digital gradient sensing (DGS) techniques to evaluate simple shear deformation of ballistic gel. The length-to-width ratio of their specimens was 2:1, which is far smaller than the recommended 10-15:1 for ensuring shear strain homogeneity [36, 37], thus causing edge-effects. In addition, only quasi-static behavior (≤ 0.04 s⁻¹) was analyzed, which is inadequate to capture the rate-dependent behavior of soft polymers [17, 38]. Zanon et al. [39] attempted to simulate quasi-static shear response of fibrous tissues by conducting single lap shear tests as outlined by Nunes [40, 41] on fiber reinforced silicone. Although the selected specimen dimensions mitigated edge effects and/or transverse buckling, the specimen mounting method involved surface abrasion and chemical treatment, which (i) can alter composition and hence the material behavior, and (ii) might not be feasible for fragile tissue specimens. Rashid et al. [42] examined the shear behavior of brain tissue under small to moderate strain rates ($\leq 120 \text{ s}^{-1}$) by using a shear device consisting of a 5 N load cell and a linear variable displacement transducer (LVDT). The use of an LVDT to measure shear plate movement, although provides a macroscopic displacement measure, does not allow verification of shear strain homogeneity in the sample and strain rate uniformity during test duration, which are two major concerns in high strain rate experiments. For example, Kwon et al. [43] demonstrated that an unsteady momentum diffusion precedes the uniform shear deformation under elevated strain rates, during which the stress-strain response extracted from an experiment does not represent constant rate material behavior. Clearly, specimen preparation, mounting of the soft and slippery tissues and bio-simulants, and validation of a uniform strain-field within the deformed regions are some of the major challenges.

To the authors' knowledge, only two high strain rate $(10^2 - 10^3 \text{ s}^{-1})$ single pulse shear experiments on soft polymers are reported in the literature. Nie et al. [44] modified the torsional split-Hopkinson pressure bar (SHPB) [45] to conduct torsion-based simple shear tests on hollow cylindrical polydimethylsiloxane (PDMS) specimens (same setup also used in [46]). While the shear strain was measured at the inner cylindrical surface from the gages bonded on the incident torsion bar, shear stress was measured at the outer surface using a torque sensor. Such torsion-based shear tests, however, do not offer a uniform stress state throughout the sample thickness as desired in any simple shear test; the shear stresses on the inner strained surface differed by $\sim 16\%$ with respect to the outer

cylindrical surface. In addition, shear strain measurement from strain gages assumed uniform stress throughout the hollow incident bar, which yields only a first order approximation. Further, their experimental method demanded establishment of a new single pressure bar torsion SHPB setup, and required two separate experiments: one for estimating momentum diffusion duration and validating strain uniformity, and another for obtaining stress-strain response. Evidently, a simpler high strain rate shear experiment, which, in a single run, is capable of both inducing and validating a constant strain rate deformation under uniform stress state, is much needed. Saraf et al. [33] conducted double-lap shear tests on simulant gels and human tissues using a modified SHPB setup. Although their use of a lap shear setup eliminated the stress non-uniformity issue present in [44], no experimental attempt was made to quantify momentum diffusion and inertia effects, which are required to determine the "wait time" after which a constant rate stress-strain response can be extracted. Analytically, a single parameter neo-Hookean (NH) model was used in the finite element analysis to obtain a wait time estimation, which is unreliable because the NH model is mathematically proven to be unsuitable for simple shear [47, 48]. Additionally, the use of tangent modulus (at shear strain $\gamma \rightarrow$ 0) from dynamic shear tests to determine the NH model constant is inaccurate because the initial material response is dominated by inertia effects and unsteady Couette flow [49]. Further, a laser-based displacement sensor was used to detect lap plate movement; thus, sample slippage along the interfaces could not be detected. None of the two aforementioned studies attempts to validate quantitatively the realization of a theoretical simple shear deformation state with uniform strain-field and strain rate during the test duration.

In this study, quasi-static and SHPB-based high strain rate simple shear experiments are developed for testing soft materials under large shear deformation (>50%) and at shear strain rates between $10^{-3}-10^{-1} \text{ s}^{-1}$ and $10^{2}-10^{3} \text{ s}^{-1}$, respectively. Cross-linked PDMS elastomer is used as a model material, which has been extensively studied for biomedical applications, such as tissue engineering scaffolds [50, 51] and biosimulants [52, 53]. For the quasi-static tests, a custom-made shear fixture is used in the standard universal testing setup, where the deformation is captured using a charge-coupled device (CCD) camera. For the high strain rate test, a custombuilt single-lap shear fixture is sandwiched between the two SHPB pressure bars. The shear load experienced by the sample is measured directly using a piezoelectric force transducer and a high-speed camera is used to capture the shear deformation. In both experiments, 2D DIC is used for full-field strain measurement on the sample surfaces, and sample dimensions are chosen based on detailed theoretical analysis to eliminate any edge effects and transverse buckling. Engineering stress, strain, and strain rate response of PDMS are extracted, enabling identification of four stages of dynamic shear



deformation. Experimental [43] and theoretical [54] results from previous studies are used to corroborate the observed transient shear behavior (momentum diffusion and inertia effect), which continues until a characteristic wait time (estimated for each test) after which a constant strain rate material response is extracted. Further, the variation of shear modulus with applied strain rate is analyzed. By comparing the experimentally observed strain-state with that of theoretical simple shear, the ability of the proposed test methods to induce a near-theoretical deformation state is demonstrated. In addition, strain uniformity in the specimen and strain rate constancy during the tests are validated.

Theoretical Background

In this section, a brief continuum mechanical description of the simple shear deformation state is presented. Both kinematic and kinetic aspects are covered, which are later used to validate the proposed experiments and to analyze stresses and strains in PDMS during simple shear.

Consider a rectangular prism geometry (dimensions: $L \times h \times d$) undergoing a simple shear deformation in the presence of a force P as shown in Fig. 1. The reference configuration, Ω_0 , under this homogeneous deformation, is mapped to the deformed configuration, Ω_x , as

$$x_1 = X_1$$

 $x_2 = X_2 + \gamma X_1$
 $x_3 = X_3$ (1)

where $\mathbf{X} = \{X_1, X_2, X_3\}$ and $\mathbf{x} = \{x_1, x_2, x_3\}$ are vectors identifying a particular material point in the reference and deformed configuration, respectively, and $\gamma = \Delta/h$ is the nominal/

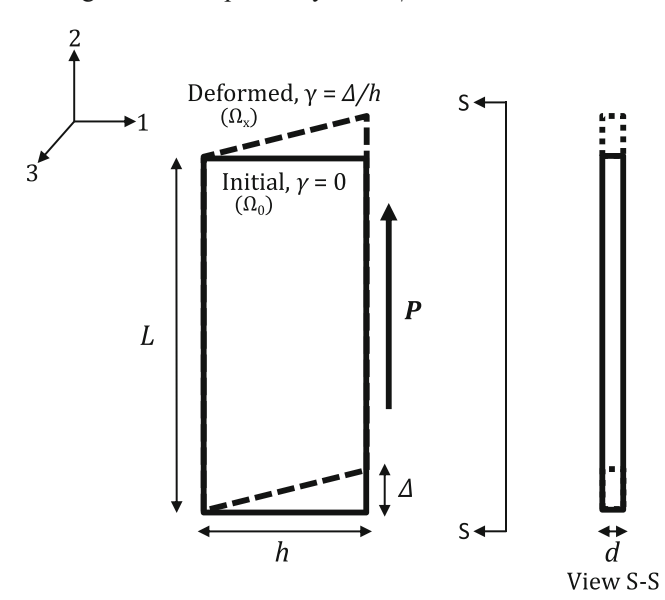


Fig. 1 Illustration of the simple shear deformation state

engineering shear strain. The deformation gradient tensor **F** is then given as.

$$\mathbf{F} = \begin{bmatrix} 1 & 0 & 0 \\ \gamma & 1 & 0 \\ 0 & 0 & 1 \end{bmatrix} \tag{2}$$

Note that simple shear deformation is *ab initio* volume preserving $(\det(\mathbf{F}) = J = 1)$. The Green-Lagrange strain tensor **E** can be calculated as

$$\mathbf{E} = \frac{1}{2} \left(\mathbf{F}^{\mathrm{T}} \mathbf{F} - \mathbf{1} \right) = \frac{1}{2} \begin{bmatrix} \gamma^2 & \gamma & 0 \\ \gamma & 0 & 0 \\ 0 & 0 & 0 \end{bmatrix}$$
 (3)

It is clear from Eq. (3) that in a classical large strain simple shear deformation, both shear strain and normal strain perpendicular to the shearing faces exist, all other strain components being zero. This fact and the fixed relationship between the two non-zero strain components in Eq. (3) are used in a later section to validate the simple shear deformation induced in the proposed experiments.

In case of dynamic shear, the rate of deformation tensor **D** is

$$\mathbf{D} = \operatorname{sym}(\mathbf{L}) = \operatorname{sym}(\dot{\mathbf{F}}\mathbf{F}^{-1}) = \frac{1}{2} \begin{bmatrix} 0 & \dot{\gamma} & 0 \\ \dot{\gamma} & 0 & 0 \\ 0 & 0 & 0 \end{bmatrix}$$
(4)

where \mathbf{D} is the symmetric part of the velocity gradient tensor $\mathbf{L} = \dot{\mathbf{F}} \mathbf{F}^{-1}$, and directly depends on the nominal shear strain rate $\dot{\gamma}$. Note that a steady-state material response can only be extracted from an experiment when the tensor \mathbf{D} in Eq. (4) is constant, in other words, when the inertia effects are nullified by zero acceleration of any material point. It is shown in the later sections that the time it takes for the tensor \mathbf{D} to attain a near-constant value in an experiment, and the duration over which it stays constant, are two major considerations in the analysis of a dynamic simple shear experimental data.

For an isotropic material, the Cauchy stress σ is written in terms of the left Cauchy-Green deformation tensor B using the Rivlin-Ericksen representation as

$$\mathbf{\sigma} = s_0 \mathbf{1} + s_1 \mathbf{B} + s_{-1} \mathbf{B}^{-1} \tag{5}$$

where **1** is the unit symmetric rank-two tensor, and s_0 , s_1 and s_{-1} are the response functions, and **B** is given as

$$\mathbf{B} = \mathbf{F} \mathbf{F}^{\mathrm{T}} = \begin{bmatrix} 1 & \gamma & 0 \\ \gamma & \gamma^2 + 1 & 0 \\ 0 & 0 & 1 \end{bmatrix}$$
 (6)

For incompressible hyperelastic (or Green-Elastic) materials such as many soft polymers [55, 56], the response functions are written in terms of the strain energy density function

 $W = W(I_1 = \gamma^2 + 3, I_2 = \gamma^2 + 3, I_3 = 1)$ as

$$s_0 = -p, s_1 = 2\left(\frac{\partial W}{\partial I_1}\right), s_{-1} = -2\left(\frac{\partial W}{\partial I_2}\right) \tag{7}$$

where p is the indeterminate hydrostatic pressure, and I_1 , I_2 , and I_3 are the principal invariants of **B**.

Using Eqs. (5) and (6), the non-zero components of σ are calculated as

$$\sigma_{11} = s_0 + s_1 + s_{-1}(\gamma^2 + 1) \tag{8.1}$$

$$\sigma_{22} = s_0 + s_1(\gamma^2 + 1) + s_{-1} \tag{8.2}$$

$$\sigma_{33} = s_0 + s_1 + s_{-1} \tag{8.3}$$

$$\sigma_{12} = (s_1 - s_{-1})\gamma \tag{8.4}$$

Equation (8) shows that unlike the pure shear deformation in which σ_{12} is the only non-zero stress component, the simple shear deformation results in a multiaxial state of both stress (Eq. (8)) and strain (Eq. (3)) with non-zero normal components. Note that the shear component is extracted experimentally as $\sigma_{12} = (P/Ld)$. Further, the initial shear modulus (measured as tangent modulus from shear experiments) is

$$\mu_0 = \lim_{\gamma \to 0} \frac{\sigma_{12}}{\gamma} \tag{9}$$

Equation (9) is used in a later section to calculate the shear modulus of PDMS at various strain rates.

Materials and Methods

Sample Preparation and Dimensions

SYLGARDTM 184 Silicone elastomer kit (Dow Silicones Corp., Midland, MI) is used as a starting material to synthesize cross-linked soft polymers in this study. The kit consists of an elastomer base and a hardener, which are thoroughly mixed in a container in 10:1 w/w ratio. The mixture is then placed inside a vacuum chamber for 2 h for degassing, wherein any air bubbles are removed as is confirmed by visual inspection. The resulting clear bubble-free viscous mixture is poured into custom-3D printed ABS (acrylonitrile butadiene styrene) polymer molds with appropriate dimensions and cured at 60 °C for three hours in an oven. Finally, cross-linked PDMS samples are taken out of the mold to conduct simple shear experiments under quasi-static and dynamic loading.

As mentioned in the "Introduction", one major challenge in designing a simple shear experiment is the selection of appropriate sample dimensions (L, h, and d) that not only ensure homogeneous deformation, but also increase the maximum observable shear strain by preventing premature sample failure. Boni et al. [57] have shown that the compressive stress

developed along the direction inclined with respect to the shearing direction may cause buckling if sample thickness (*d*) is very small. Accordingly, the condition of no buckling suggested in [58] is modified for incompressible hyperelastic materials as

$$\frac{d}{h} > \frac{1}{\pi} \sqrt{\frac{\tau_c}{3\mu_o}} \tag{10}$$

where τ_c is the maximum shear stress experienced by the sample during the test, and μ_o is the tangent shear modulus. Preliminary shear experiments on PDMS samples of varying dimensions suggested that both τ_c and μ_o are approximately 0.5 MPa (similar numbers reported in [40, 41]). Equation (10) thus becomes

$$\frac{d}{h} > 0.18 \tag{11}$$

Another challenge in simple shear testing is to overcome the inherent edge effects (stress inhomogeneity at sample edges) caused by the normal stresses originating from grip constraints. G'Sell and Boni [36], considering a first-order approximation of the varying constraint stresses $\overline{\sigma}_N$, proposed

$$\frac{L}{h} > 0.75 \frac{\sigma_{12}}{\left| \overline{\sigma_N} \right|} \tag{12}$$

To ensure that the unwanted normal stresses are at least an order of magnitude smaller than the applied shear stress,

$$\frac{L}{h} > 7.5 \tag{13}$$

Accordingly, the gage section dimensions for quasi-static and dynamic test specimens are selected as 40 mm (L) × 3.5 mm (h) × 3.5 mm (d) and 45 mm (L) × 4.5 mm (h) × 3.5 mm (d), respectively, thus satisfying both the Eqs. (11) and (13) with a good margin. Note that the overall specimen width h is greater than the gage section width h to accommodate mounting plates: h = 35 mm and 30 mm for quasi-static and dynamic test samples, respectively. An illustration of specimen dimensions is presented in Figs. 2 and 3.

Quasi-Static Experimental Setup

All quasi-static tests are conducted on a dual column electromechanical universal testing machine (Frame 311, TestResources, Inc., Shakopee, MN) equipped with a 1.1 kN load cell (\pm 0.5% accuracy). A custom-built single-lap shear fixture is used as shown in Fig. 2, which consists of two L-shaped plates (Lap-1 and Lap-2). A PDMS specimen sheet (40 mm \times 35 mm \times 3.5 mm) is glued on the side faces of the lap plates using a 1:10 v/v dispersion of N-butyl cyanoacrylate adhesive (Vetbond tissue adhesive, 3 M, St. Paul, MN) in 1-

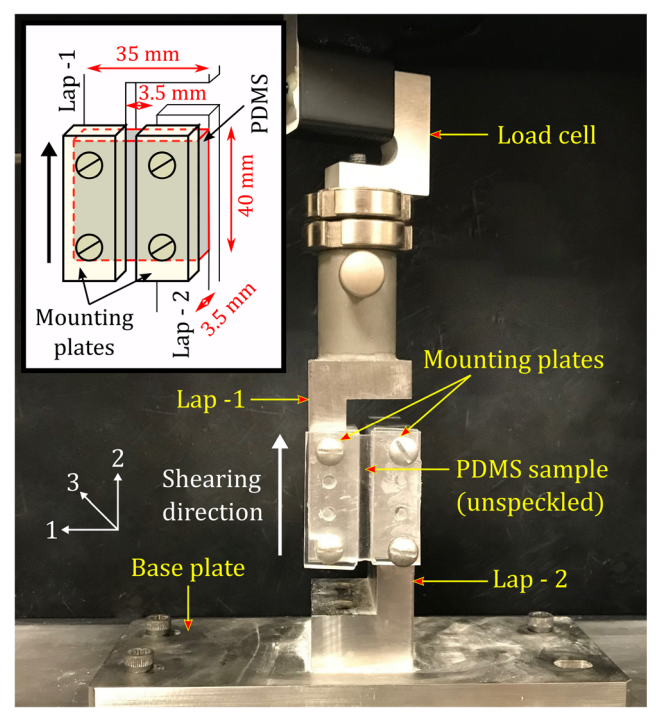


Fig. 2 Quasi-static simple shear test setup. The inset shows a schematic of the mounting assembly with specimen and gage section dimensions shown in red

Octadecene (Fisher Scientific, Fair Lawn, NJ) non-solvent [59]. This dispersion is ideal for the test because (i) cyanoacrylate-based adhesives result in strong bonds [37], (ii) polymerize rapidly (< 1 min) so that the curing reaction

is confined to a very thin layer (~100 µm) [60], and (iii) the alkene-based dispersion prevents formation of brittle acrylic resins at the metal-polymer interface [59], which can otherwise lead to premature sample failure. To constrain and support the front sample faces that are separated by its gage section (3.5 mm width), a thin layer of adhesive dispersion is applied to two mounting plates that further clamp the specimen against the two lap plates. Note that a low clamping force is maintained by controlling screw thread rotation to ensure negligible out-of-plane strains in the gage section (verified separately using 3D DIC). All tests are conducted in displacement-controlled mode by translating Lap-1 (or crosshead) vertically at appropriate velocities (velocity $\dot{\Delta} = h\dot{\gamma}$) in order to impart shear strain at a desired strain rate in the PDMS sample gage section. Three tests are conducted at each strain rate level of 10^{-3} , 10^{-2} , and 10^{-1} s⁻¹.

2D DIC is used for strain measurement, which is a noncontact optical method that maps planar strain-fields by tracking the movement of a randomly distributed speckle pattern on a sample surface. Fine chalk powder (100–200 μ m) is used to create a random and homogeneous pattern on the sample gage area, which is then imaged during deformation at regular intervals using a 5.0 MP CCD camera (GRAS-50S5M-C (Sony ICX 625 CCD), FLIR Sytems, Inc., Richmond, Canada). The pixel resolution is 2448 × 2048 pixels and the spatial resolution is ~40 pixels/mm, such that around 140 pixels exist along the width of the specimen gage section. Acquired images are analyzed using the commercial VIC-2D 6 software (Correlated Solutions, Inc., Irmo, SC); subset

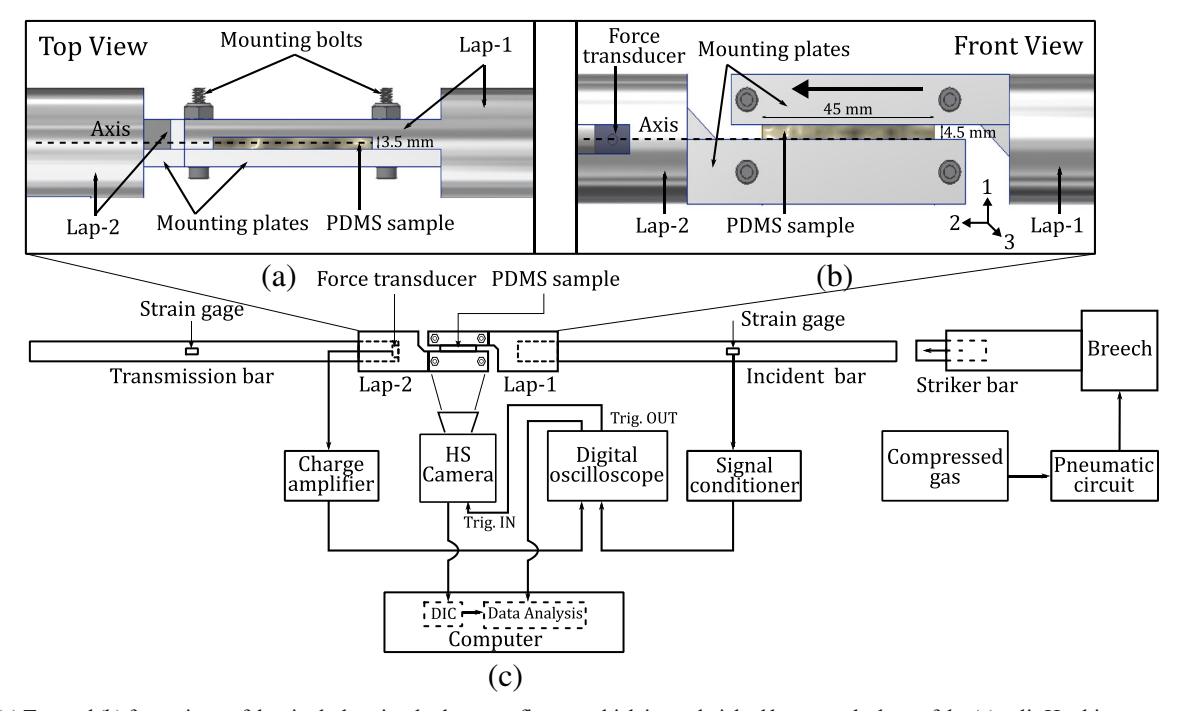


Fig. 3 (a) Top and (b) front views of the single-lap simple shear test fixture, which is sandwiched between the bars of the (c) split-Hopkinson pressure bar apparatus

size is selected for individual imaging data based on the speckle density and size (subset size $> (3 \times \text{speckle size})$), and also the sigma value (one standard deviation confidence interval) of the subset tracking function.

Dynamic Experimental Setup

Simple shear tests at strain rates in the order of 10^2-10^3 s⁻¹ are conducted using a modified SHPB. A detailed schematic of the experimental setup is shown in Fig. 3, which consists of two long cylindrical maraging steel bars known as the incident and the transmission bars on which strain gages are centrally bonded; a shorter striker bar slides inside a long barrel connected to a pressurized nitrogen gas chamber. A single-lap shear test fixture, which houses the PDMS specimen between its individual Lap-1 and Lap-2 parts, is inserted between the two pressure bars through its hollow cylindrical ends (see Fig. 3(c)). A PDMS specimen plate (45 mm \times 30 mm \times 3.5 mm) is glued to the lap faces using the same cyanoacrylate-alkene adhesive dispersion used in quasi-static testing. To ensure a no-slip condition, two mounting plates are used to further secure the specimen against the individual laps. This ensures that the sample gage section (4.5 mm width) experiences simple shear as Lap-1 translates relative to Lap-2 (see Figs. 3(a) and (b)). The gage section is speckled by fine black spray paint (Krylon Products Group, Cleveland, OH) (100-300 µm); no base coat was applied as it may stiffen the material. A charge-output force transducer (Model 210B, PCB Piezotronics, Inc., Depew, NY) is sandwiched between the transmission bar and Lap-2 to sense the shear force experienced by the specimen. The deformation event is captured using a high-speed camera (Phantom v710, Vision Research, Inc., Wayne, NJ) capable of capturing images at up to 1.4 million frames per second (fps). Signal output from strain gages, force transducer, and high-speed camera are processed through an array of different signal processing equipment. Eight tests are conducted at different strain rates ranging between 10^2 and 10^3 s⁻¹.

To start the experiment, pressurized gas from a compressed gas cylinder is used to launch the striker bar toward the incident bar; the resulting impact generates a compressive stress (and so strain) wave. The strain gage mounted on the incident bar measures this transient strain signal, which is recorded as voltage signal in the digital oscilloscope (MSO-X 3034A, Agilent Technologies, Inc., Colorado Springs, CO) after passing through a signal-conditioning amplifier (2310B, Micro-Measurements, Inc., Rayleigh, NC). When the stress wave reaches the incident bar end, it imparts a high velocity input to Lap-1, causing simple shear deformation of the sample. Figure 4 shows a characteristic ideal velocity profile of the incident bar end, which is a rectangular pulse of width $T = 2l_s/C_b$ ($l_s = 152.5$ mm and $C_b = 4975$ m/s are striker bar length and the incident bar 1D stress wave velocity, respectively) and

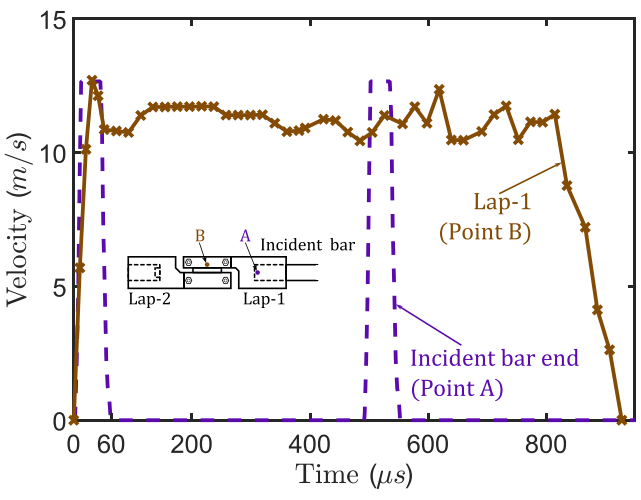


Fig. 4 Particle velocity versus time plot for the incident bar end and Lap-1. Inset shows a schematic of the dynamic shear fixture, where points A and B are labelled to show locations where velocity was measured/estimated for the incident bar end and Lap-1, respectively

a peak value $v_{ib, max} = 2C_b\varepsilon_{I, max}$ ($\varepsilon_{I, max}$ is the recorded peak incident strain). In addition, the velocity of Lap-1 (at point A) in the same test is shown, which is measured from the highspeed images using the MTrackJ plugin [61] of the ImageJ freeware [62]. Note that the two velocity profiles diverge after the first wave reaches its peak, suggesting that Lap-1 separates from the incident bar after this point due to their sliding fit with respect to each other, and that the former (Lap-1) traverses with roughly a constant velocity (~12 m/s in this case) for several hundred microseconds. Soft polymers such as PDMS have a very low impedance as compared to metallic pressure bars, and thus most of the stress wave reflects back into the incident bar. The role of the SHPB apparatus is thus to only provide a constant velocity impulse to the Lap-1 of the single lap shear fixture, while the Lap-2 remains stationary because only an insignificant portion of the original stress wave passes through the specimen to reach the transmission bar. The shear force experienced by the sample is measured by the force transducer, providing charge signals to the charge amplifier/converter (Type 5010B, Kistler Instrument Corp., Amherst, NY), which converts the charge signal into an amplified voltage signal suitable for recording by the digital oscilloscope. The fixture dimensions are such that both the shear plane and center plane along sample thickness pass through the force transducer axis, eliminating any unwanted bending moment. The rising voltage signal from the force transducer assembly is also used to trigger the high-speed camera through a 5 V transistor-transistor logic (TTL) pulse, synchronizing the camera imaging with force measurement. Note that the delay caused by factors such as trigger filter time (set as 32 µs), shutter speed, and exposure time, although small as compared to the total test duration, is accounted for in the subsequent analysis. The high-speed camera is set to capture deformation images at 97,000 frames per second (one image



every 10.31 μ s with an exposure time of 6.3 μ s), which yields a 512 \times 128 pixel resolution and a \sim 21 pixels/mm spatial resolution such that around 95 pixels exist along the specimen gage section width. Captured images are later analyzed in the commercial 2D DIC Vic-2D 6 software (Correlated Solutions, Inc., Irmo, SC) to measure strains and strain rates.

Results and Discussion

In this section, both qualitative and quantitative aspects of the simple shear response of PDMS are discussed, along with a detailed validation of the proposed experiments. The first two subsections discuss characteristic quasi-static and dynamic shear behavior using a typical test result from each regime. A strain rate sensitivity discussion follows in the third subsection, in which test data from multiple tests is presented. Finally, the last two subsections validate the deformation state and strain-field uniformity.

Quasi-static Simple Shear Response of PDMS

Figure 5 shows a characteristic quasi-static engineering shear stress versus strain plot as extracted from a 10^{-3} s⁻¹ strain rate experiment; 2D DIC engineering shear strain maps are constructed from deformed sample images captured every 3 s, and are shown at 0.1 mm/mm strain increments. The stress-strain response is linear until a large strain limit of $\gamma = 0.46$, after which there is visible slippage between sample gage section corners and grips, where strain inhomogeneity is maximum (see shear strain-field maps corresponding to $\gamma = 0.5$ and 0.6 in Fig. 5). Note that this strain limit is caused by an experimental factor and does not represent actual material behavior; it also varies between individual tests.

Fig. 5 Engineering shear stress versus strain plot for a quasi-static simple shear test at 10^{-3} s⁻¹ strain rate, with engineering shear strain-field maps at every 0.1 mm/mm strain step. Deformation images after the large strain limit of $\gamma = 0.46$ show significant slippage in regions highlighted by red boxes

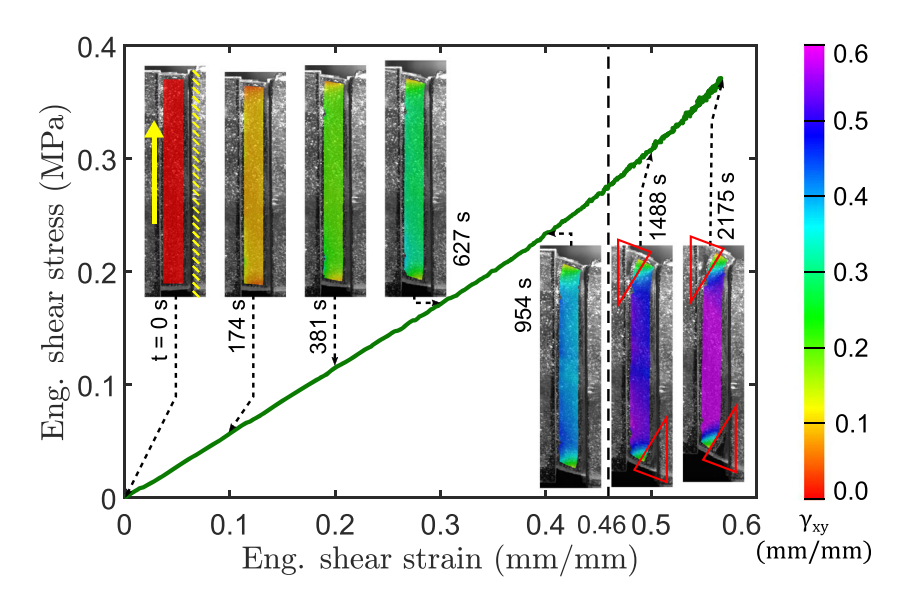
All experiments in the present work are displacement controlled; the stabilization of the Lap-1 velocity is thus critical for capturing a steady-state material response. In the quasistatic test, this rise time of crosshead speed from zero to a constant value is negligible as compared to the total test duration (2175 s in Fig. 5). Thus, the rate of deformation tensor **D** (Eq. (4)) is a constant and consequently, the entire stress-strain response represents material behavior at a constant strain rate.

High Strain Rate Simple Shear Response of PDMS

Figure 6(a) shows a characteristic simple shear response as determined from the modified SHPB experiment. Four distinct stages of the dynamic simple shear deformation are identified from this figure:

Stage I - Momentum diffusion (Couette flow)

Kwon et al. [43] showed that high strain rate simple shear tests on soft polymers involve a delay between the times when Lap-1 starts moving and when the stationary Lap-2 feels the shear force. In Fig. 6(a), this is the 144 us delay between the initial rise of strain and stress responses, which corresponds to the first three deformation images in Fig. 6(a). The transient momentum diffusion can be modelled using a non-Newtonian power law fluid model which, for a linearly ramping velocity input (such as the one in SHPB), leads to a one-to-one relation between diffusion length and time regardless of the applied strain rate [43]. Figure 7 plots the momentum diffusion time between Lap-1 and Lap-2 as a function of strain rate for eight dynamic tests. Note that time required for the stress wave to travel from specimen end to load cell through the aluminum Lap-1 is \sim 7 µs, which is smaller than the 10.31 µs resolution of strain measurement, and thus is neglected. Recall, the lap



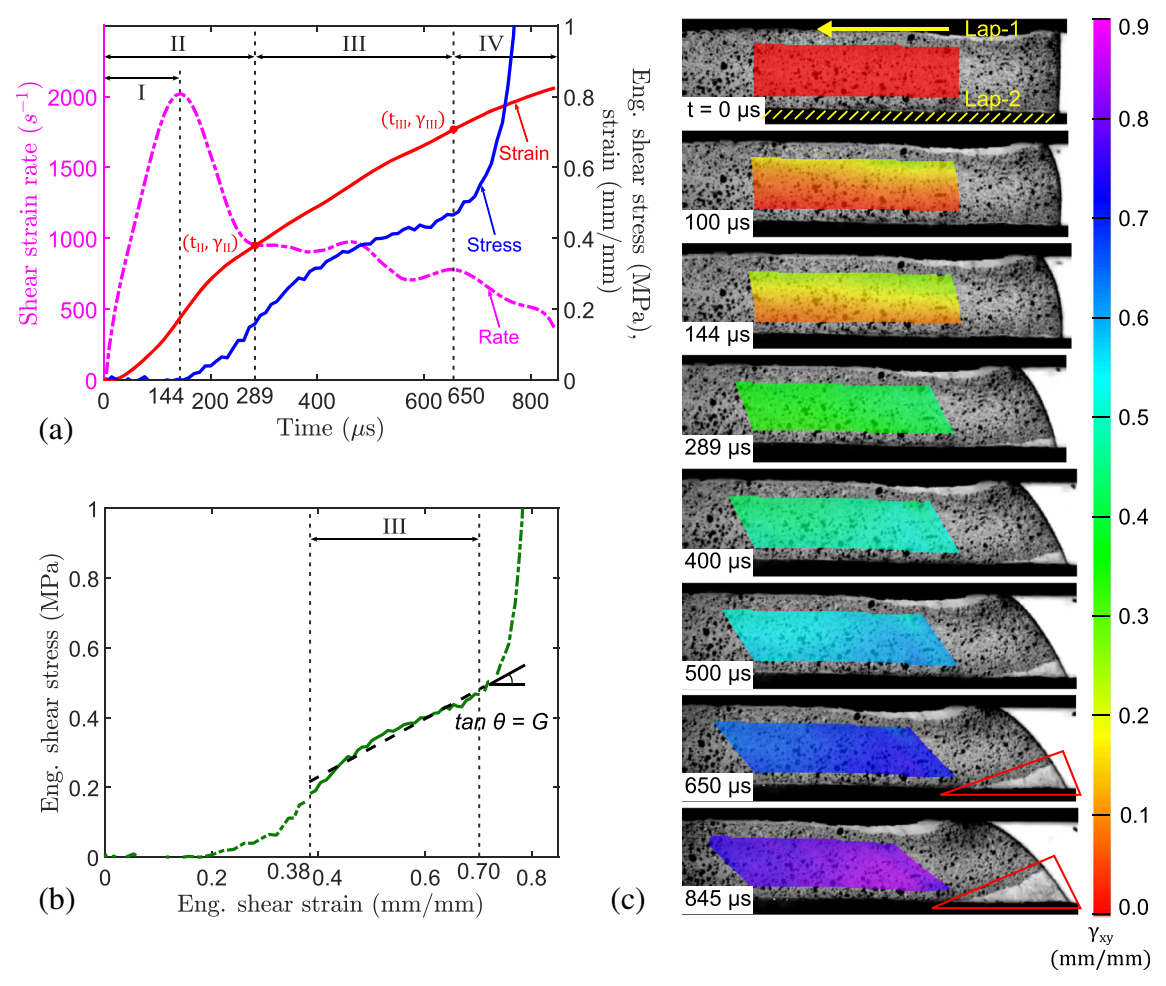


Fig. 6 (a) Evolution of stress, strain, and strain rate with respect to time in a typical dynamic simple shear experiment, showing four stages of deformation: I - Momentum diffusion, II - Inertia effect, III - Steady-state material response, and IV - Strain rate decay. (b) Engineering shear stress versus strain plot with highlighted stage III, which is used to calculate shear modulus G. (c) Deformed sample images showing engineering shear strain field (central and right-side regions of the specimen are captured); last two images show significant slippage in regions highlighted by red boxes

plates are separated by a constant distance of \sim 4.5 mm (see Fig. 3(b)). The experimentally observed transient response

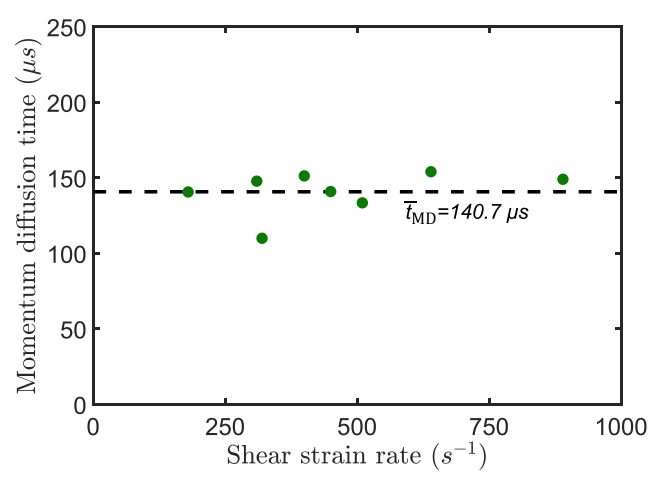


Fig. 7 Momentum diffusion time as a function of applied strain rate in dynamic simple shear experiments

conforms to the theoretical momentum diffusion behavior, yielding a near-constant diffusion time $t_{MD} = 140.7 \pm 11.9 \,\mu s$ (p value <0.05) regardless of strain rate.

Stage II - Inertia effect

Stage II corresponds to a rapid rise and fall in the strain rate (0 to 289 μ s in Fig. 6(a); first four deformation images in Fig. 6(c)). Unlike the constant duration momentum diffusion stage (for a fixed sample width) that depends solely on the non-Newtonian material flow behavior, the strain rate rise in stage II corresponds to the experimentally controllable characteristic SHPB pulse width; for example, a longer striker bar results in a longer rise time. Unlike the compression SHPB experiment in which the strain rate remains constant for a finite duration after reaching its peak, in the dynamic shear experiment, Lap-1 disconnects from the incident bar for the rest of the test duration after this strain rate rise caused during its initial propulsion. Therefore, the fall in strain rate after the

initial rapid rise is mainly due to the inertia offered by the polymer sample material. Overall, stage II corresponds to the duration in which strain-acceleration is significantly large, and thus material response is dominated by the inertia effect. The longer duration among stages I and II is the wait time, t_{wait}

$$t_{wait} = \max(t_{MD}, t_{IE}) \tag{14}$$

where t_{MD} and t_{IE} denote the duration of the momentum diffusion and inertia effect stages. Note that t_{wait} depends on both material properties and the experimental setup (e.g., specimen width, striker bar length, etc.), and thus does not change with the applied strain rate. It is only after the wait time that the experimental data represents a steady-state material behavior, which can be used to obtain stress-strain response at a specific strain rate. For the typical dynamic experiment shown in Fig. 6, $t_{wait} = 289 \,\mu s$. Note that in the present study, as the specimen width is kept small to eliminate edge effects, t_{IE} is always greater than t_{MD} , making the former equal to the wait time in every test. However, if the specimen width is large enough, the time for momentum diffusion to occur can be comparable or longer than that to achieve a constant strain rate response.

Gilchrist et al. [54] recently proposed a theoretical rateindependent time upper bound for which inertial effects are significant in a strain-controlled experiment

$$t_{IE}^{th} = h\sqrt{\frac{\rho}{S}} \tag{15}$$

where t_{IE}^{th} denotes the theoretical estimation of inertia effect duration, h is the specimen width in simple shear, ρ is the mass density, and S is the maximum shear stress experienced by the specimen during a particular test. Note that Eq. (15) is applicable only if the following condition is satisfied

$$\max\{Q_h, Q_v\} \ll 1 \tag{16}$$

where Q_h and Q_v are non-dimensional parameters given by

$$Q_h = \frac{\rho(\dot{\gamma}h)^2}{S}; Q_\nu = \frac{\rho}{\nu} \left(\frac{h}{S}\right)^2 \tag{17}$$

In Eq. (17), γ is the average strain rate applied during the test, and ν is the slope of S versus γ plot. Table 1 summarizes the theoretical estimates of the duration when inertia effect is dominant for the eight dynamic shear experiments conducted, along with Q_h and Q_ν parameter values and the experimentally observed wait (or inertia effect) times for the same experiments; test numbers are organized in increasing order of strain rate.

Table 1 shows that the non-dimensional parameters Q_h and Q_ν are at least an order of magnitude smaller than unity for every high strain rate SHPB experiment, making the theoretical estimation of wait time using Eq. (15) valid. Further, the theoretical wait time for every test is smaller than the

Table 1 Comparison of the theoretically estimated time upper bound of dominant inertia effects with the experimentally observed values

Test no.	Strain rate (s ⁻¹)	Q_h	Q_{ν}	t_{IE}^{th} (µs)	t _{wait} (µs)
1	180	0.002	0.037	255	258
2	310	0.005	0.043	237	289
3	320	0.004	0.056	193	237
4	400	0.006	0.054	195	232
5	450	0.010	0.052	217	247
6	510	0.011	0.055	202	227
7	640	0.015	0.060	193	247
8	890	0.034	0.053	207	289

experimentally observed duration, suggesting that Eq. (15) yields a more conservative estimation of inertia effect duration than the actual value. This can be useful in cases where measurement of wait time using a strain rate versus time plot is difficult or not possible. In addition, as the wait time stays constant regardless of the applied strain rate, the strain at the end of stage II increases for higher strain rates, eventually leading to a situation where the test finishes without the sample ever attaining a steady-state response. This can also be seen from the increasing values of Q_h with strain rate; $Q_h \gtrsim$ 0.1 renders the entire test duration overwhelmed with inertia effects [54]. Therefore, a steady-state material response cannot be extracted beyond a certain limiting strain rate. This limiting strain rate can be increased by reducing the sample width h, which in turn is limited by experimental constraints such as speckle size in DIC and sample preparation, among others. Nevertheless, the results and analysis in the present study take into account the various unsteady phenomena of stages I and II, and report only the material response under steady-state.

Stage III - Steady-state material response

In stage III, the sample deforms under a nearly constant strain rate (289 to 650 μ s in Fig. 6(a); fourth to seventh deformation image in Fig. 6(c)). The average strain rate $\bar{\gamma}$ is calculated as

$$\frac{\overline{\dot{\gamma}}}{\dot{\gamma}} = \frac{\gamma_{III} - \gamma_{II}}{t_{III} - t_{II}} \tag{18}$$

where subscripts *II* and *III* denote that their respective time and nominal shear strain values are measured at the end of stages II and III, respectively (see Fig. 6(a)). Figure 6(b) plots the engineering shear stress versus strain response of a PDMS sample, where stage III response (solid line) represents the constant rate material behavior whose linear regression slope provides the shear modulus. Further, the average strain rate calculated from Eq. (18) is referred to as the applied strain rate in dynamic experiments, and is used to study the strain rate sensitivity of the shear modulus of PDMS in a later section. Note that the frame interval of high-speed imaging results in a

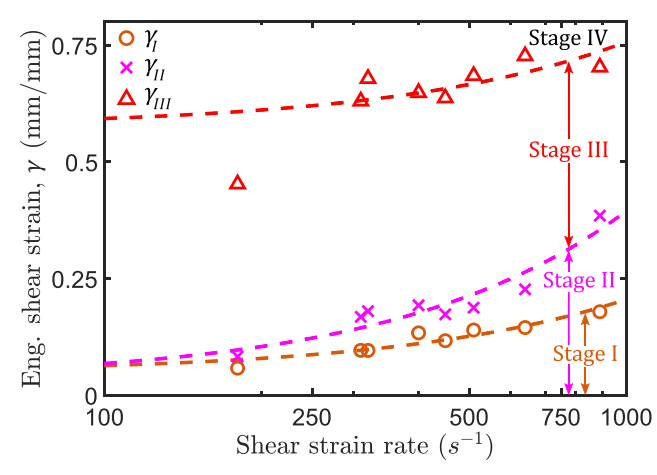


Fig. 8 Engineering shear strain at the end of various deformation stages as a function of applied strain rate for dynamic (eight) simple shear experiments

time uncertainty of 10.31 μs in strain measurement corresponding to a particular stress value. To ascertain the effect of this uncertainty, the stress curve in Fig. 6(a) is shifted $\pm 5.16~\mu s$ on either side of its current position, and the shear modulus is recalculated. The resulting variation in the shear modulus is less than $\pm 2.3\%$. Thus, the error due to the temporal resolution of strain is very small, and can be safely neglected.

Stage IV - Strain rate decay

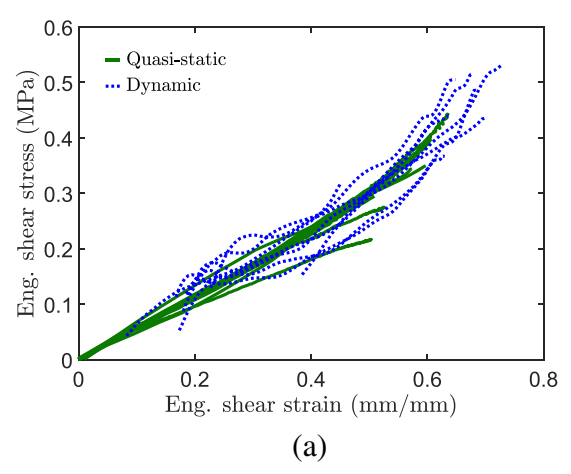
The final stage (650 to 845 μ s in Fig. 6(a); last two images in Fig. 6(c)) corresponds to the plateauing of the strain-time response followed by a rapid fall. This can be caused by a number of factors: (i) specimen failure, (ii) translation of Lap-2 as sufficient shear force accumulates, and (iii) impact between Lap-1 and Lap-2 as the gap between them closes under large shear. The latter factor causes a sudden rise in shear stress measured by the force transducer (Fig. 6(b)), after

which the deformation diverges from a simple shear mode and the sample-grip slippage becomes excessive (see Fig. 6(c)). In addition, significant inertia effects arise due to large negative strain acceleration. Therefore, this stage should be disregarded in the study of a steady-state material response.

It is clear that the steady-state material response in a dynamic simple shear experiment can only be extracted in the stage III of deformation, i.e., when material follows static equilibrium and thus deforms at a constant rate and under a uniform strain-field. Figure 8 plots the nominal shear strain at the end of stages I, II and III (denoted as γ_I , γ_{II} and γ_{III} , respectively) as observed in dynamic shear tests at different strain rates. Although the time durations corresponding to stages I and II remain constant with strain rate, the strains γ_I and γ_{II} for a fixed material and SHPB setup increase because deformation occurs at faster rates. Strain γ_{III} , on the other hand, increases but is bounded by the failure shear strain of the material. Therefore, the stage III steady-state response observation window shrinks with strain rate, which limits the experimentally achievable steady-state strain rate in dynamic simple shear experiments. Note that experimental factors such as smaller specimen width (h) and a shorter striker bar can lead to smaller γ_I and γ_{II} values, thus expanding the stage III observation window. In addition, a stronger adhesive mounting and an increased gap between Lap-1 and Lap-2 can also be implemented to optimize stage III duration.

Shear Strain Rate Sensitivity of PDMS

Figure 9(a) shows the engineering shear stress versus strain response as obtained from the quasi-static and high strain rate experiments. As mentioned in the preceding section, while the quasi-static stress-strain data starts from the origin, the high strain rate steady-state material response is obtained only in the stage III window (see Fig. 6(b)); thus, the dynamic stress-



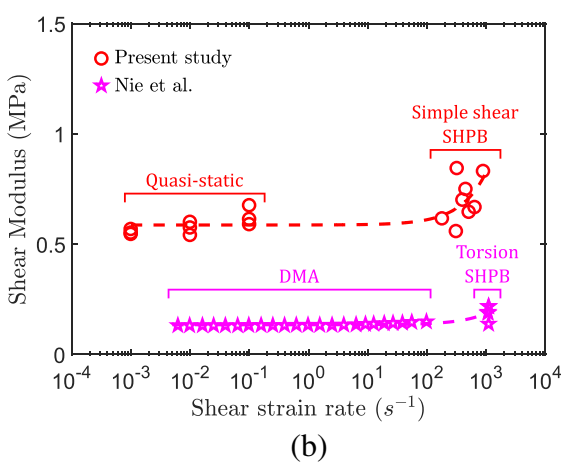


Fig. 9 (a) Engineering shear stress versus strain plot for quasi-static (nine) and dynamic (eight) simple shear experiments. (b) Variation of shear modulus with strain rate as observed in the present work, and its comparison with the results obtained by Nie et al. [44] on PDMS of unspecified base to hardener ratio



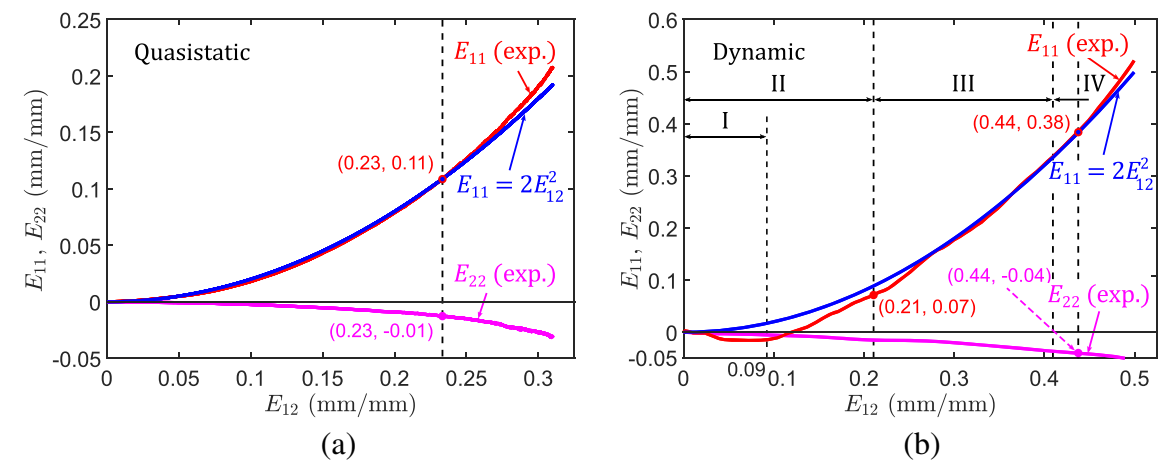


Fig. 10 Deformation state validation in (a) quasi-static and (b) dynamic shear experiments using Green-Lagrangian strain tensor components. In both cases, the experimentally measured E_{11} strain follows the ideally quadratic relationship (Eq. (19)) with the shear strain E_{12} during steady-state deformation; E_{22} strain component is an order of magnitude smaller than both E_{11} and E_{12} ($E_{22} \approx 0$ for $E_{12} < 0.1$)

strain data shown in Fig. 9(a) does not start from the origin. Regardless of the strain rate, the stress-strain response is nearly linear up to certain large strain limit, after which specimengrip slippage becomes excessive so that simple shear conditions no longer hold. This suggests that the slope at any point before this limit represents the initial shear modulus of the material (linear regression is used for dynamic test plots).

Figure 9(b) plots the shear modulus as a function of the applied shear strain rate, and compares it with the results obtained in [44], where small strain DMA and dynamic torsion SHPB experiments were conducted on PDMS samples of unspecified base to cross-linker ratio. The results of the present study reveal that the shear modulus of PDMS (10:1 w/w, base to hardener) in the quasi-static regime is 0.58 ± 0.03 MPa, which increases slightly beyond 10^2 s⁻¹ strain rate in the

dynamic regime to 0.70 ± 0.08 MPa (p value <0.05). Further, linear regression analysis results in a positive slope of $2.41 \times 10^{-4} \pm 1.31 \times 10^{-4}$ MPa/s (p value <0.05), suggesting a weak dependence of shear modulus on strain rate. Similar trend was reported by Nie et al. [44] as shown in Fig. 9(b), where the average shear modulus of 0.14 MPa resulted by DMA increased to 0.19 MPa under high strain rate shear conditions. Also, an increased data scatter in the latter regime was observed.

Thus far, it has been demonstrated that the proposed experiments achieve a finite duration window of constant strain rate response (stage III in Fig. 6(a)), thus enabling extraction of an inertia free material behavior. The next two subsections validate the other two essential conditions: (i) deformation state is simple shear, and (ii) strain-field in the specimen is uniform.

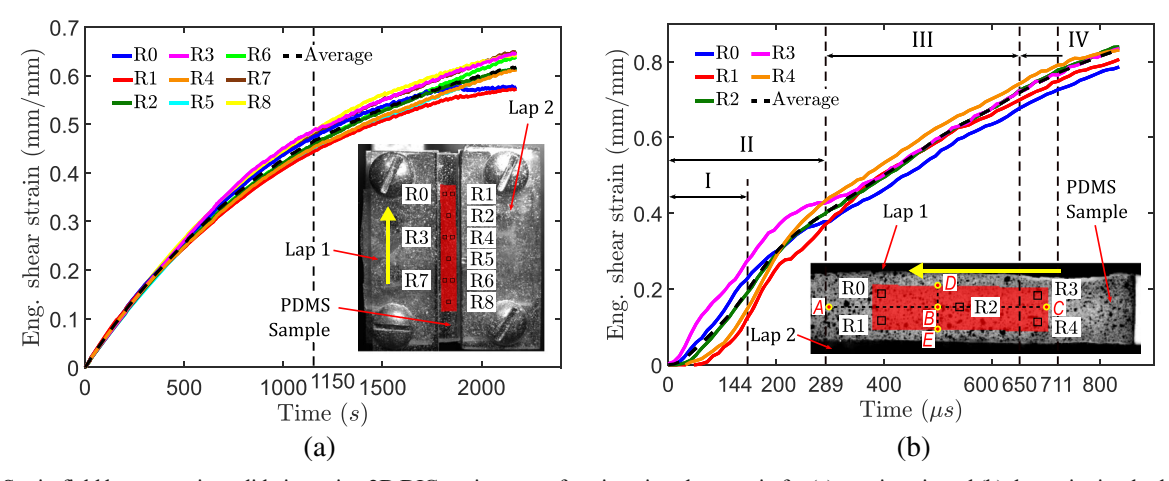


Fig. 11 Strain-field homogeneity validation using 2D DIC strain maps of engineering shear strain for (a) quasi-static and (b) dynamic simple shear tests. Nine (R0 through R8) square areas are analyzed for the quasi-static tests; five (R0 through R4) square areas are analyzed for the dynamic tests. Inset shows images of sample gage sections with Lap-1 and Lap-2 plates just before the test, and highlighted central regions that are analyzed using DIC. The shear strain along the two line segments (vertical (D-E) and horizontal (A-C) median) in the inset of (b) are investigated in Fig. 12

Deformation State Validation

Equation (3) in the "Theoretical Background" section suggests that for a theoretical simple shear deformation state, the 1–2 and 1–1 components of the Green-Lagrange strain tensor ${\bf E}$ are first and second order in the engineering shear strain γ , respectively, all other components being zero. Therefore, the following relation exists between its two nonzero components:

$$E_{11} = 2(E_{12})^2 (19)$$

Note that Eq. (19) holds when the shear force acts on the 1-2 plane and toward \mathbf{e}_2 direction (see Fig. 1); coordinate systems for quasi-static and dynamic experimental analysis are accordingly defined as shown in Figs. 2 and 3(b), respectively.

Figures 10(a) and (b) show plots of E_{11} and E_{22} versus E_{12} strain components as extracted from the 2D DIC analysis of a characteristic quasi-static and high strain rate experiment, respectively. In the quasi-static case (Fig. 10(a)) in which the entire test occurs at a constant rate under steady-state conditions, the experimental E_{11} strain component is in excellent agreement with its theoretical prediction from Eq. (19) until certain large shear strain value of $E_{12} = 0.23$ ($\gamma = 0.46$ in Fig. 5). As mentioned in the preceding sections, after this limit is reached, the slippage between the sample gage section edges and grips becomes excessive, and the stress-strain response of PDMS becomes non-linear (see Fig. 5).

On the other hand, the dynamic case (Fig. 10(b)) involves a wait time owing to the initial unsteady momentum diffusion (stage I) and inertia effects (stage II). Therefore, the initial average experimental E_{11} in these stages diverges from the classical continuum mechanical prediction, which assumes an equilibrium homogeneous simple shear condition. For the characteristic dynamic test discussed in this work, stages I and II end at 144 µs and 289 µs, respectively (see Fig. 6(a)), which

corresponds to Lagrangian strain components $E_{12} = 0.09$ ($\gamma = 0.19$) and $E_{12} = 0.21$ ($\gamma = 0.40$), respectively. In Fig. 10(b), starting from $E_{12} = 0.21$ and up to a large strain limit of $E_{12} = 0.44$ ($\gamma = 0.77$), there is an excellent agreement between the experimental and theoretical E_{11} values. Note that the entire stage III deformation occurs concurrently with a nearly theoretical simple shear state in the sample, further corroborating the validity of the results.

Furthermore, the E_{22} strain component in both quasi-static and dynamic cases is close to zero for shear strains (E_{12}) less than 0.1, and beyond this value, E_{22} remains an order of magnitude smaller than the two non-zero strain components (E_{11} and E_{12}), thus exhibiting reasonable agreement with the theory. Clearly, the proposed testing methods simulate the simple shear deformation state reasonably well.

Strain-Field Homogeneity Validation

Figures 11(a) and (b) plot the evolution of engineering shear strain with time at several distinct small areas throughout the central and side regions of the sample gage sections in a quasistatic and a dynamic shear experiment, respectively. In the former case, nine square regions labeled R0 through R8 are analyzed. The strain evolution shows a nearly uniform strain distribution until the large strain limit of $E_{12} = 0.23$ mentioned in Fig. 10(a) (corresponding to 1150 s in Fig. 11(a)), with a maximum deviation of 4.81% with respect to average strain.

For the dynamic shear case, five square regions labeled R0 through R4 in the central and right-side regions of the specimen (images capture \sim 55% of the total specimen length)) are analyzed (Fig. 11(b)). Similar to theoretical simple shear realization, the strain-field exhibited homogeneity (max. Deviation 8.33% relative to the average strain) in a time window that started after the completion of wait time (289 μ s) and up to the time corresponding to the large strain limit in

Fig. 12 Shear strain variation along the horizontal (A-C) and vertical (D-E) line segments on the sample surface (shown in the inset of Fig. 11(b)) at different times during the course of the dynamic simple shear experiment; x-axis is the normalized distance, with 0 representing the left (A) and top (D) ends, and 1 representing the right (C) and bottom (E) ends of the horizontal and vertical segments, respectively

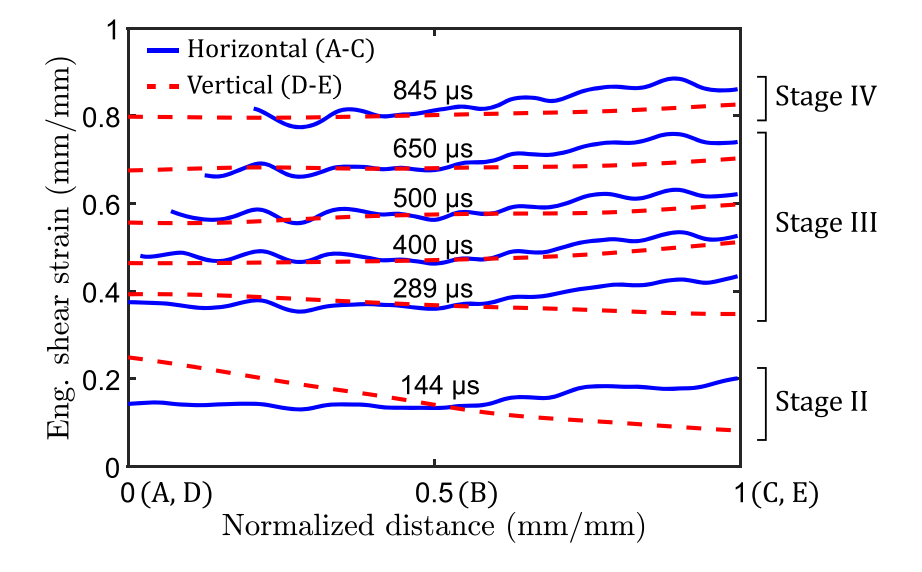


Fig. 10(b), i.e., 711 µs. Further, the variation of shear strain along two line-segments shown in the inset of Fig. 11(b) (vertical (D-E), and horizontal median (A-C) of the analyzed area) is investigated at different times during the experiment (Fig. 12). Consistent with the definition of the various stages of dynamic shear deformation defined in Fig. 6, there is a high strain non-uniformity and a steadily decreasing shear strain along the vertical line during the transient stage II. The strain fields are uniform during the steady-state deformation (stage III). The maximum absolute deviation in the steady-state shear strain with respect to the average value is 4.28% and 8.05% for the vertical and horizontal segments, respectively. Not surprisingly, the strain-field exhibits a better homogeneity in the central region of the sample (near point A), which is apparent from the maximum shear strain deviation of only 1.56% across the half-segment A-B. The slightly increased variation of shear strain between points B and C causes reduction in homogeneity from 1.56% to 8.05%. Overall, the proposed dynamic shear test ensures that the entire stage III (289 to 650 µs) deformation in the specimen occurs when the shear strain-field is homogeneous.

Conclusion

Simple shear experiments on soft polymers involve major challenges: (i) sample mounting and preparation, (ii) application of a wide range of constant strain rates and (iii) large shear deformation under a single pulse loading, (iv) maintaining strain-field uniformity, and (v) identifying and capturing steady-state material response. The present study overcomes these challenges via the development of quasi-static and SHPB based high strain rate single-lap shear experiments rooted in continuum mechanics principles. In both tests, specimens are sandwiched between shear lap and mounting plates using a cyanoacrylate-based adhesive dispersion, which allows large slip-less shear deformation without interfering with material composition. Specimen dimensions are carefully chosen to mitigate edge effects and transverse buckling, resulting in a uniform strain-field that is later validated using 2D DIC. A constant crosshead velocity is set in the quasistatic test to ensure constant strain rate deformation. In dynamic tests, the SHPB provides a high rate loading pulse leading to a constant strain rate sample deformation for several microseconds duration. Full-field strain measurement allows extraction of the Green-Lagrangian strain components, which exhibit excellent agreement with those predicted using classical continuum mechanics; thus, a nearly theoretical simple shear deformation is achieved. From the dynamic experiments, four stages of simple shear deformation are identified: (i) momentum diffusion, (ii) inertia effect, (iii) steady-state material response, and (iv) strain rate decay. Transient and steady-state deformation regimes are delineated in individual tests, allowing selective capture of constant strain rate material response. Thus, by using standard quasi-static and dynamic uni-axial test setups retrofitted with custom-made test fixtures, simple and inexpensive simple shear experiments with individual test validation capability are developed.

The stage I of dynamic simple shear, the momentum diffusion, is due to the transient startup Couette flow of PDMS under high strain rates, which is confirmed by the constant diffusion time versus strain rate response, as suggested in the literature. The inertia effect (stage II) corresponds to a large strain acceleration. The longer stage among the first two yields the wait time, after which the experimental data represents actual material response under a constant strain rate (stage III) until the initiation of the ultimate strain rate decay (stage IV). It is shown that the experimentally determined wait time agrees with a recently proposed mathematical equation for predicting durations in which inertia effects are dominant, the latter yielding a slightly conservative estimate in most cases. Further, it is shown that the stage III observation window shrinks with increasing strain rate, allowing a smaller strain range to be analyzed; stage III duration can be optimized by using a smaller specimen width and a shorter striker bar.

By conducting multiple quasi-static and dynamic experiments on PDMS elastomers, it is demonstrated that the simple shear response of PDMS is nearly linear elastic. In addition, a weak strain rate sensitivity with respect to shear modulus is observed. Thus, in addition to allowing observation of a wider range of dynamic strain rates with a simple experiment under uniform and large shear, the present results agree qualitatively with the small-strain DMA and torsion SHPB findings in the literature. Finally, the rate-independent stress-strain response suggests applicability of hyperelastic strain-energy density based constitutive relations to describe the mechanical behavior of PDMS, which will be pursued in future work.

Acknowledgements This research was supported by the National Science Foundation under Grant Nos. CMMI-1634188 and CMMI-1762791 to the University of Florida, Gainesville, USA.

References

- Roberts JC, Merkle AC, Biermann PJ et al (2007) Computational and experimental models of the human torso for non-penetrating ballistic impact. J Biomech 40:125–136. https://doi.org/10.1016/j. jbiomech.2005.11.003
- Merkle AC, Ward EE, O Connor JV, Roberts JC (2008) Assessing Behind Armor Blunt Trauma (BABT) Under NIJ Standard-0101.04 Conditions Using Human Torso Models. J Trauma Inj Infect Crit Care 64:1555-1561. https://doi.org/10.1097/TA. 0b013e318160ff3a
- Chatelin S, Deck C, Willinger R (2013) An anisotropic viscous hyperelastic constitutive law for brain material finite-element

- Joldes GR, Wittek A, Miller K (2009) Suite of finite element algorithms for accurate computation of soft tissue deformation for surgical simulation. Med Image Anal 13:912–919. https://doi.org/10.1016/i.media.2008.12.001
- Groves RB, Coulman SA, Birchall JC, Evans SL (2013) An anisotropic, hyperelastic model for skin: Experimental measurements, finite element modelling and identification of parameters for human and murine skin. J Mech Behav Biomed Mater 18:167–180. https://doi.org/10.1016/j.jmbbm.2012.10.021
- Misra S, Ramesh KT, Okamura AM (2008) Modeling of Tool-Tissue Interactions for Computer-Based Surgical Simulation: A Literature Review. Presence Teleoperators Virtual Environ 17: 463–491. https://doi.org/10.1162/pres.17.5.463
- Jennifer M, Cronin DS, Worswick M, et al (2001) Numerical Modelling of a Simplified Surrogate Leg Subject To an Anti-Personnel Blast Mine. In: Proceedings of the 19th International Symposium of Ballistics. Interlaken, pp 913–919
- Kohandel M, Sivaloganathan S, Tenti G, Darvish K (2005) Frequency dependence of complex moduli of brain tissue using a fractional Zener model. Phys Med Biol 50:2799–2805. https://doi. org/10.1088/0031-9155/50/12/005
- Parnaik Y, Beillas P, Demetropoulos CK et al (2004) The influence of surrogate blood vessels on the impact response of a physical model of the brain. Stapp Car Crash J 48:259–277
- Doorly MC, Gilchrist MD (2006) The use of accident reconstruction for the analysis of traumatic brain injury due to head impacts arising from falls. Comput Methods Biomech Biomed Engin 9: 371–377. https://doi.org/10.1080/10255840601003551
- Kleiven S (2007) Predictors for traumatic brain injuries evaluated through accident reconstructions. Stapp Car Crash J 51:81–114
- Harrigan TP, Roberts JC, Ward EE, Merkle AC (2010) Correlating Tissue Response with Anatomical Location of mTBI Using a Human Head Finite Element Model under Simulated Blast Conditions. In: IFMBE Proceedings. pp 18–21
- Normand V, Lootens DL, Amici E et al (2000) New insight into agarose gel mechanical properties. Biomacromolecules 1:730–738. https://doi.org/10.1021/bm005583j
- Miller K (2005) Method of testing very soft biological tissues in compression. J Biomech 38:153–158. https://doi.org/10.1016/j. jbiomech.2004.03.004
- Forte AE, Galvan S, Manieri F et al (2016) A composite hydrogel for brain tissue phantoms. Mater Des 112:227–238. https://doi.org/ 10.1016/j.matdes.2016.09.063
- Pervin F, Chen WW (2009) Dynamic mechanical response of bovine gray matter and white matter brain tissues under compression. J Biomech 42:731–735. https://doi.org/10.1016/j.jbiomech.2009.01.023
- Naarayan SS, Subhash G (2017) Wave propagation in ballistic gelatine. J Mech Behav Biomed Mater 68:32–41. https://doi.org/10.1016/j.jmbbm.2017.01.030
- Subhash G, Liu Q, Moore DF et al (2011) Concentration Dependence of Tensile Behavior in Agarose Gel Using Digital Image Correlation. Exp Mech 51:255–262. https://doi.org/10. 1007/s11340-010-9354-2
- Singh A, Lu Y, Chen C, M Cavanaugh J (2006) Mechanical properties of spinal nerve roots subjected to tension at different strain rates. J Biomech 39:1669–1676. https://doi.org/10.1016/j.ibiomech.2005.04.023
- Shim VPW, Liu JF, Lee VS (2006) A Technique for Dynamic Tensile Testing of Human Cervical Spine Ligaments. Exp Mech 46:77–89. https://doi.org/10.1007/s11340-006-5865-2
- Yang LM, Shim VPW, Lim CT (2000) A visco-hyperelastic approach to modelling the constitutive behaviour of rubber. Int J Impact Eng 24:545–560. https://doi.org/10.1016/S0734-743X(99) 00044-5

- Sasson A, Patchornik S, Eliasy R et al (2012) Hyperelastic mechanical behavior of chitosan hydrogels for nucleus pulposus replacement-Experimental testing and constitutive modeling. J Mech Behav Biomed Mater 8:143–153. https://doi.org/10.1016/j.imbbm 2011.12.008
- Rashid B, Destrade M, Gilchrist MD (2014) Mechanical characterization of brain tissue in tension at dynamic strain rates. J Mech Behav Biomed Mater 33:43–54. https://doi.org/10.1016/j.jmbbm. 2012.07.015
- Ogden RW (1972) Large Deformation Isotropic Elasticity: On the Correlation of Theory and Experiment for Compressible Rubberlike Solids. Proc R Soc A Math Phys Eng Sci 328:567– 583. https://doi.org/10.1098/rspa.1972.0096
- Ogden RW, Saccomandi G, Sgura I (2004) Fitting hyperelastic models to experimental data. Comput Mech 34:484–502. https:// doi.org/10.1007/s00466-004-0593-y
- Upadhyay K, Subhash G, Spearot D (2019) Thermodynamics-based stability criteria for constitutive equations of isotropic hyperelastic solids. J Mech Phys Solids 124:115–142. https://doi.org/10.1016/j.jmps.2018.09.038
- Arbogast KB, Thibault KL, Scott Pinheiro B et al (1997) A high-frequency shear device for testing soft biological tissues. J Biomech 30:757–759. https://doi.org/10.1016/S0021-9290(97)00023-7
- Bilston LE, Liu Z, Phan-Thien N (2001) Large strain behaviour of brain tissue in shear: some experimental data and differential constitutive model. Biorheology 38:335–345
- Bercoff J, Tanter M, Fink M (2004) Supersonic shear imaging: a new technique for soft tissue elasticity mapping. IEEE Trans Ultrason Ferroelectr Freq Control 51:396–409. https://doi.org/10. 1109/TUFFC.2004.1295425
- Jiang Y, Li G, Qian L-X et al (2015) Measuring the linear and nonlinear elastic properties of brain tissue with shear waves and inverse analysis. Biomech Model Mechanobiol 14:1119–1128. https://doi.org/10.1007/s10237-015-0658-0
- Nasseri S, Bilston LE, Phan-Thien N (2002) Viscoelastic properties of pig kidney in shear, experimental results and modelling. Rheol Acta 41:180–192. https://doi.org/10.1007/s003970200017
- Hrapko M, van Dommelen JAW, Peters GWM, Wismans JSHM (2008) Characterisation of the mechanical behaviour of brain tissue in compression and shear. Biorheology 45:663–676. https://doi.org/ 10.3233/BIR-2008-0512
- Saraf H, Ramesh KT, Lennon AM et al (2007) Measurement of the Dynamic Bulk and Shear Response of Soft Human Tissues. Exp Mech 47:439

 –449. https://doi.org/10.1007/s11340-007-9052-x
- 34. Trexler MM, Lennon AM, Wickwire AC et al (2011) Verification and implementation of a modified split Hopkinson pressure bar technique for characterizing biological tissue and soft biosimulant materials under dynamic shear loading. J Mech Behav Biomed Mater 4:1920–1928. https://doi.org/10.1016/j.jmbbm.2011.06.008
- Pasumarthy RKA, Tippur HV (2016) Mechanical and optical characterization of a tissue surrogate polymer gel. Polym Test 55:219
 229. https://doi.org/10.1016/j.polymertesting.2016.08.004
- G'Sell C, Boni S, Shrivastava S (1983) Application of the plane simple shear test for determination of the plastic behaviour of solid polymers at large strains. J Mater Sci 18:903–918. https://doi.org/ 10.1007/BF00745590
- Subhash G, Kwon J, Mei R, Moore DF (2012) Non-Newtonian Behavior of Ballistic Gelatin at High Shear Rates. Exp Mech 52: 551–560. https://doi.org/10.1007/s11340-011-9513-0
- Van Sligtenhorst C, Cronin DS, Wayne Brodland G (2006) High strain rate compressive properties of bovine muscle tissue determined using a split Hopkinson bar apparatus. J Biomech 39: 1852–1858. https://doi.org/10.1016/j.jbiomech.2005.05.015
- Zanon AG, Cardoso PN, Moreira CS, da Silva Nunes LC (2015) Mechanical behavior of silicone rubber reinforced with parallel fibers of nylon under simple shear: a study on artificial soft tissue.

- Proceedings of the 23rd ABCM International Congress of Mechanical Engineering, Rio de Janeiro
- Nunes LCS (2011) Mechanical characterization of hyperelastic polydimethylsiloxane by simple shear test. Mater Sci Eng A 528: 1799–1804. https://doi.org/10.1016/j.msea.2010.11.025
- Nunes LCS (2010) Shear modulus estimation of the polymer polydimethylsiloxane (PDMS) using digital image correlation. Mater Des 31:583–588. https://doi.org/10.1016/j.matdes.2009.07.012
- Rashid B, Destrade M, Gilchrist MD (2013) Mechanical characterization of brain tissue in simple shear at dynamic strain rates. J Mech Behav Biomed Mater 28:71–85. https://doi.org/10.1016/j.imbbm.2013.07.017
- Kwon J, Subhash G, Mei R, Heger I (2011) An optical technique for determination of rheological properties of gelatin. J Rheol (N Y N Y) 55:951–964. https://doi.org/10.1122/1.3599676
- Nie X, Prabhu R, Chen WW et al (2011) A Kolsky Torsion Bar Technique for Characterization of Dynamic Shear Response of Soft Materials. Exp Mech 51:1527–1534. https://doi.org/10.1007/ s11340-011-9481-4
- Gilat A (2000) Torsional Kolsky Bar Testing. Mater Park OH ASM Int 2000 505–515
- Sanborn B, Nie X, Chen W, Weerasooriya T (2012) High Strain Rate Pure Shear and Axial Compressive Response of Porcine Lung Tissue. J Appl Mech 80:011029. https://doi.org/10.1115/1.4007222
- Puglisi G, Saccomandi G (2016) Multi-scale modelling of rubber-like materials and soft tissues: An appraisal. Proc R Soc A Math Phys Eng Sci 472:20160060. https://doi.org/10.1098/rspa.2016.0060
- Saccomandi G (2018) Ut vis sic tensio. Theor Appl Mech 45:1–15. https://doi.org/10.2298/TAM170703011S
- Nie X, Song B, Ge Y et al (2009) Dynamic Tensile Testing of Soft Materials. Exp Mech 49:451–458. https://doi.org/10.1007/s11340-008-9133-5
- Pedraza E, Brady A-C, Fraker CA, Stabler CL (2013) Synthesis of macroporous poly(dimethylsiloxane) scaffolds for tissue engineering applications. J Biomater Sci Polym Ed 24:1041–1056. https:// doi.org/10.1080/09205063.2012.735097
- Mohanty S, Larsen LB, Trifol J et al (2015) Fabrication of scalable and structured tissue engineering scaffolds using water dissolvable

- sacrificial 3D printed moulds. Mater Sci Eng C 55:569–578. https://doi.org/10.1016/j.msec.2015.06.002
- Payne T, Mitchell S, Halkon B et al (2016) Development of a synthetic human thigh impact surrogate for sports personal protective equipment testing. Proc Inst Mech Eng Part P J Sport Eng Technol 230:5–16. https://doi.org/10.1177/1754337115582294
- Payne T, Mitchell S, Bibb R, Waters M (2015) The evaluation of new multi-material human soft tissue simulants for sports impact surrogates. J Mech Behav Biomed Mater 41:336–356. https://doi. org/10.1016/j.jmbbm.2014.09.018
- Gilchrist MD, Rashid B, Murphy JG, Saccomandi G (2013) Quasistatic deformations of biological soft tissue. Math Mech Solids 18: 622–633. https://doi.org/10.1177/1081286513485770
- Wex C, Arndt S, Stoll A et al (2015) Isotropic incompressible hyperelastic models for modelling the mechanical behaviour of biological tissues: A review. Biomed Tech 60:577–592. https:// doi.org/10.1515/bmt-2014-0146
- Mihai LA, Budday S, Holzapfel GA et al (2017) A family of hyperelastic models for human brain tissue. J Mech Phys Solids 106:60–79. https://doi.org/10.1016/j.jmps.2017.05.015
- 57. Boni S, G'Sell C, Weynant E, Haudin JM (1982) Microscopic in situ observation of the plastic deformation of polybutene-1 films under simple shear. Polym Test 3:3–24. https://doi.org/10.1016/0142-9418(82)90009-5
- Bleich F (1952) Buckling strength of metal structures, 1st edn. McGraw-Hill, New York
- Wirthl D, Pichler R, Drack M et al (2017) Instant tough bonding of hydrogels for soft machines and electronics. Sci Adv 3:1–10. https://doi.org/10.1126/sciadv.1700053
- Wang M, Komfield JA (2012) Measuring shear strength of softtissue adhesives. J Biomed Mater Res Part B Appl Biomater 100B: 618–623. https://doi.org/10.1002/jbm.b.31981

Publisher's Note Springer Nature remains neutral with regard to jurisdictional claims in published maps and institutional affiliations.